Bioorganic & Medicinal Chemistry 17 (2009) 5572–5582

Contents lists available at ScienceDirect

Bioorganic & Medicinal Chemistry

journal homepage: www.elsevier.com/locate/bmc

Identification of potential cellular targets of aloisine A by affinity chromatography

Caroline Corbel [a], Rose Haddoub [b], Damien Guiffant [a], Olivier Lozach [a], David Gueyrard [b], Jérôme Lemoine [c,*], Morgane Ratin [a], Laurent Meijer [a], Stéphane Bach [a,*], Peter Goekjian [b,*]

[a] CNRS USR-3151, Protein Phosphorylation and Human Disease, Station Biologique, B.P.74, F-29682 Roscoff Cedex, Bretagne, France
[b] Université de Lyon, CNRS UMR 5246 ICBMS, Laboratoire de Chimie Organique 2—Glycochimie, Université Claude Bernard Lyon 1, CPE-Lyon, Bâtiment 308, 43 Boulevard du 11 Novembre 1918, Villeurbanne F-69622, France
[c] Université de Lyon, CNRS UMR 5180, Université Claude Bernard Lyon 1, Bâtiment 308, 43 Boulevard du 11 Novembre 1918, Villeurbanne F-69622, France

ARTICLE INFO

Article history:
Received 6 February 2009
Revised 5 June 2009
Accepted 14 June 2009
Available online 18 June 2009

Keywords:
Aloisine
Immobilized protein kinase inhibitor
Mass spectrometry
Click chemistry
Pyrrolo[2,3-*b*]pyrazine
Cyclin-dependent kinase
Pyridoxal kinase
Affinity chromatography
GSK-3
Fuse binding protein 1
Glycogen-debranching enzyme
ERK1

ABSTRACT

Affinity chromatography was used to identify potential cellular targets of aloisine A (7-*n*-butyl-6-(4′-hydroxyphenyl)-*5H*-pyrrolo[2,3*b*]pyrazine), a potent inhibitor of cyclin-dependent kinases. This technique is based on the immobilization of the drug on a solid matrix, followed by identification of specifically bound proteins. To this end, both aloisine A and the protein-kinase inactive control *N*-methyl aloisine, bearing extended linker chains have been synthesized. We present the preparation of such analogues having the triethylene glycol chain at different positions of the molecule, as well as their immobilization on an agarose-based matrix. Affinity chromatography of various biological extracts on the aloisine matrices allowed the identification of both protein kinases and non-kinase proteins as potential cellular targets of aloisine.

© 2009 Elsevier Ltd. All rights reserved.

1. Introduction

Cyclin-dependent kinases (CDKs) are low-molecular-weight serine-threonine kinases that require association to a regulatory subunit, a cyclin, in order to be activated. CDKs play important roles in the cell division cycle, apoptosis, differentiation, neuronal functions, and transcription.[1–3] Abnormalities and dysregulations of CDK activities have been associated with many diseases including cancers, viral infections, ischemia, and neurodegenerative disorders such as Alzheimer's and Parkinson's disease.[4] Recent data have notably implicated CDK5 in aberrant tau phosphorylation and the association of the latter with microtubules. Hyperphosphorylation, aggregation, and formation of the filamentous form of tau protein (paired helical filaments or PHF-Tau) are all observed in Alzheimer's disease but also in other diseases referred to as neurodegenerative tauopathies.[5] Furthermore, cyclin-dependent kinases are conserved across species during evolution, providing new insights and new pharmacological opportunities for the treatment of infectious diseases. These observations have encouraged an intensive search for potent and selective pharmacological inhibitors of CDKs. A large number of small molecular weight inhibitors have been characterized to date, all of which appear to act by direct competition with ATP.[6–8]

The selectivity of kinase inhibitors is usually addressed by testing the inhibitor against a panel of purified kinases.[9] But even for the largest panels, these only reflect a fraction of the 518 kinases that constitute the human kinome. In addition, the chemical compound might interact with some of the other ~1500 ATP utilizing enzymes and numerous other nucleotide-binding proteins present in the human proteome. As a consequence many of the potential targets are not evaluated using this method which, in addition, requires time- and budget- consuming expression, purification and assay set up for each individual kinase. Finally, in vitro assay against recombinant enzymes may not adequately reflect the distribution or the phosphorylation states found in vivo. This

* Corresponding authors. Fax: +33 472448319 (J.L.); fax: +33 298292526 (S.B.); fax: +33 478898914 (P.G.).
E-mail addresses: jerome.lemoine@univ-lyon1.fr (J. Lemoine), bach@sb-roscoff.fr (S. Bach), goekjian@univ-lyon1.fr (P. Goekjian).

0968-0896/$ - see front matter © 2009 Elsevier Ltd. All rights reserved.
doi:10.1016/j.bmc.2009.06.024

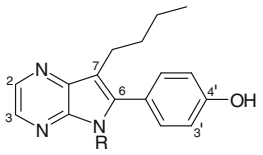

Scheme 1. Structure of aloisine A (R = H) and *N*-methyl-aloisine A (R = Me).

method, although useful to give a first idea about the selectivity of such ATP-competitive inhibitors, is thus clearly not comprehensive. Using this approach, the exact mechanism of action and the full spectrum of their targets remain largely unknown. Determination of the in vivo selectivity and identification of their intracellular targets is a prerequisite in order to understand their cellular effects and to improve their efficiency on a rational basis. Different approaches have therefore been developed to study the spectrum of in vivo intracellular targets.[10,11] In particular the purification of intracellular targets by affinity chromatography using immobilized drugs[12] has been applied successfully notably to the study of purvalanol,[13] paullones,[14] hymenialdisine,[15] Iressa[16] and roscovitine.[17]

In this paper, we report the results of our investigation on the targets of aloisine A. Aloisine A (7-*n*-butyl-6-(4′-hydroxyphenyl)-5*H*-pyrrolo[2,3-*b*] pyrazine) is a potent inhibitor of CDKs,[18] whereas its *N*-methyl derivative is completely inactive (Scheme 1). In vitro assays have shown that aloisine A is highly selective for CDK1/cyclin B, CDK2/cyclin A-E, CDK5/p25 and GSK-3, the two latter enzymes being implicated in Alzheimer's disease. Moreover this drug displays antiproliferative activity thus warranting further investigation of its selectivity for a better understanding of its cellular and physiological action and optimization of its pharmacological properties. To this aim, we have designed aloisine A analogues conjugated with a linker suitable for immobilization onto a matrix and used them for the purification of the cellular targets of aloisine A. Finally, we have investigated the activity of aloisine A against targets from simpler organisms, such as budding yeast cdk's and the *Plasmodium falciparum* homologue of GSK-3.

2. Results

2.1. Design

A triethylene glycol (TEG) chain was selected as a linker for immobilization due to its hydrophilic properties which allow a good presentation of the inhibitor with minimal unfavorable folding on the matrix and non-specific adsorption of proteins. Furthermore, the linker was introduced to avoid possible steric hindrance between target(s) and the matrix.[12] From a chemical point of view, either the NH of the pyrrolo[2,3-*b*]pyrazine ring or the hydroxyl group of the phenol moiety can be functionalized directly with the linker. The crystal structure of aloisine A complexed to CDK2/5 shows that the NH group is involved in a key hydrogen-bond with the protein, whereas the 4′-OH group points out of the ATP binding cleft and is not involved in any specific interactions.[18,19] The butyl chain at the C-7 position is pointing toward a small hydrophobic pocket, but may be accessible in other target proteins. Crystal structure and QSAR studies have also shown that modifications on the C-2 and C-3 of the pyrazine core lead to a decrease of the inhibition activity of the aloisine A.

We thus decided to introduce a linker on the positions 4′, 3′, and 7 for our investigations. Although one can anticipate a slight perturbation in the biological activity of aloisine A by such modifications, the combined affinity profiles of the differently linked compounds should give a fairly complete view of the potential enzymatic targets of aloisines. The *N*-methyl analogues (substitution of the hydrogen atom in position 5 by a methyl group) were also prepared as negative controls as this substitution results in a dramatic decrease in the protein kinase inhibitory activity.[18]

2.2. Synthesis

2.2.1. Synthesis of aloisine A analogues with a linker at the 4′-OH position

The synthesis of the pyrrolo[2,3-*b*]pyrazine core is typically performed by condensation between an alkylpyrazine and a benzonitrile derivative.[20] Introduction of the linker in the 4′-OH position can be performed either before or after the condensation step. As the condensation is the limiting step and proceeds in moderate yield, we decided to introduce the linker at an early stage (Scheme 2). Therefore, 4-hydroxybenzonitrile was reacted with the monotosylated triethylene glycol **1** in the presence of potassium carbonate in DMF to obtain **2** in 75% yield. The aloisine core was then prepared by condensation of **2** with *n*-pentylpyrazine according to the literature with a slight modification. Indeed, initial attempts of condensation provided the expected product in low yield. Further investigations revealed that an excess of LDA was required for the formation of the pyrrolo[2,3-*b*]pyrazine ring **3** in acceptable yield, presumably via to the formation of a dianion intermediate.[21] The protected alcohol was then converted into an amine suitable for coupling with the agarose-based matrix. To this end, compound **3** was treated with a catalytic amount of *p*-toluenesulfonic acid (*p*-TSA) in methanol to afford the corresponding alcohol. Iodination by treatment with triphenylphosphine/imidazole/iodine in DMF followed by displacement with sodium azide gave the corresponding alkyl azide which, in turn, yielded the primary amine **5** upon hydrogenation. Methylation of **3** with methyl iodide and sodium hydride gave the *N*-methyl analog **4**, which after an identical sequence of reactions, gave the *N*-methyl control compound **6** in similar yields.

2.2.2. Synthesis of aloisine A analogues with a linker at the C-7 position

In order to introduce the linker at the C-7 position, the strategy was again to synthesize a pyrazine core conjugated with the TEG, followed by condensation with the appropriate benzonitrile derivative. Synthesis of the pyrazinyl derivative was achieved by alkylation between 2-methyl pyrazine and the chain **7**[22] to afford the desired pyrazinyl derivative **9** in 46% yield (Scheme 2). However, attempts at condensation with 4-methoxybenzonitrile gave yields between 5% and 15%. We reasoned that these disappointing results may be due to a complexation of the lithium by the TEG chain (e.g., structure **A**), thus hampering its reaction with the benzonitrile derivative. We therefore decided to synthesize a longer chain with the hope to prevent this complexation phenomenon. Briefly, compound **1**[14] was substituted with 1-pentenol in the presence of sodium hydride in DMF to give the corresponding ether in 56% yield. Ozonolysis, reduction with sodium borohydride, tosylation, and iodination gave the extended chain iodide **8**, which was subsequently converted to the pyrazine **10**. We were delighted to observe that in this case, the expected pyrrolo[2,3-*b*]pyrazine core **11** was formed in 45% yield. The amino-functionalized aloisine derivative **12** was obtained by following the same route as described above. The *N*-methyl analogue was not prepared in this case.

2.2.3. Synthesis of aloisine A analogues with a linker at the C-3′ position

Our initial strategy was to introduce the linker by a Sonogashira coupling of an alkynyl-substituted triethyleneglycol chain with a bromobenzonitrile derivative, followed by condensation with

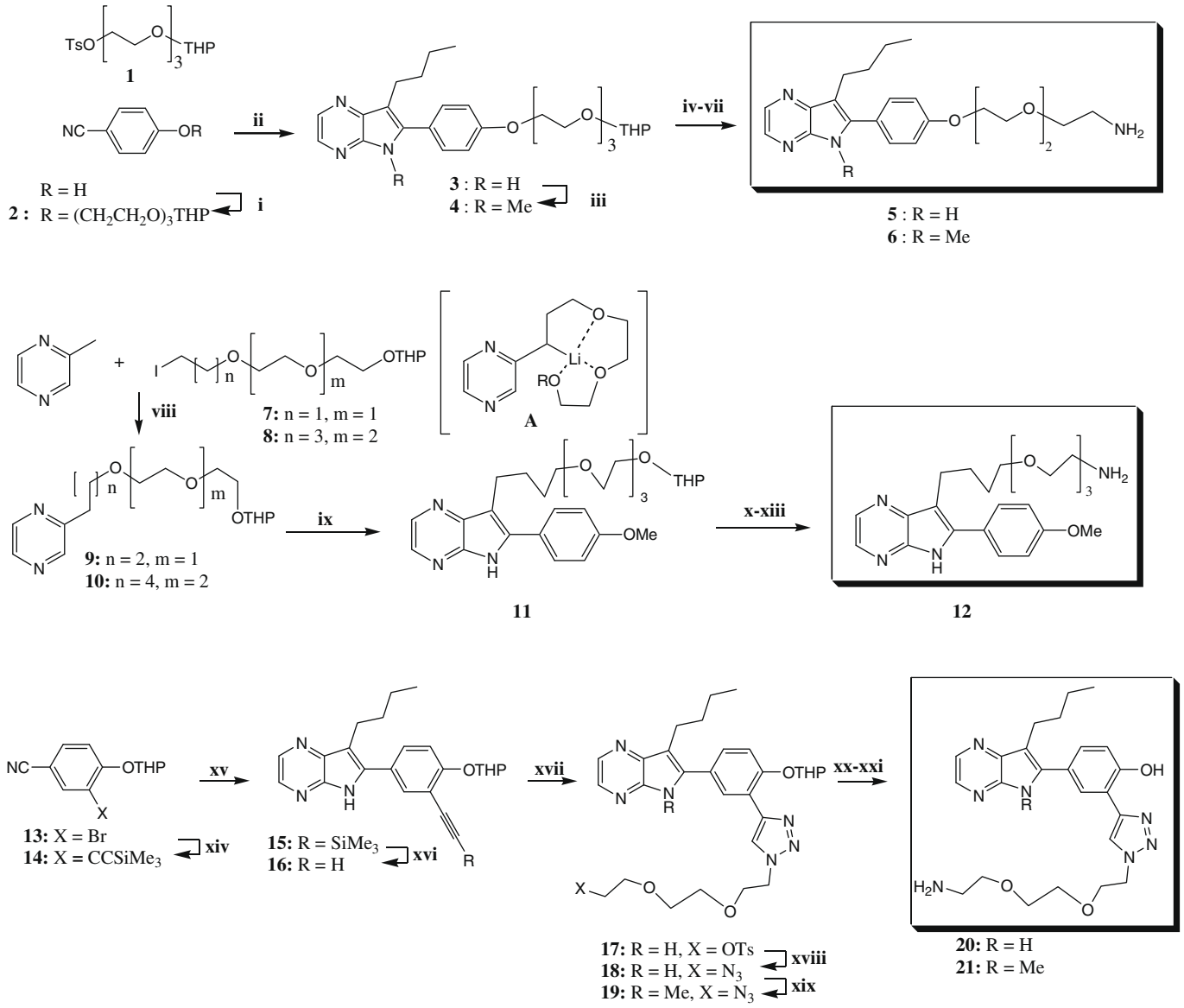

Scheme 2. Synthesis of aloisine A and *N*-methyl aloisine A analogs bearing sidechains for conjugation. (i) K_2CO_3, **1**, DMF, 60 °C (75%); (ii) LDA, *n*-pentylpyrazine, THF, −40 °C (55%); (iii) CH_3I, NaH, DMF (67%); (iv) *p*-TSA, MeOH, rt (83% R = H, 86% R = CH_3); (v) I_2, PPh_3, imidazole, DMF, 60 °C (40% R = H, 39% R = CH_3); (vi) NaN_3, DMF, 70 °C (70% R = H, 69% R = CH_3); (vii) H_2, 10%Pd/C, MeOH, rt (62% R = H, 66% R = CH_3); (viii) 2-methylpyrazine, LDA, THF, −45 °C (46%); (ix) LDA, THF, −45 °C, then 4-methoxybenzonitrile (45%); (x) TsOH, MeOH, rt (83%); (xi) I_2, TPP, imidazole, DMF, 70 °C (39%); (xii) NaN_3, DMF, 70 °C (73%); (xiii) H_2, 10%Pd/C, MeOH, rt (52%); (xiv) PPh_3, $PdCl_2(PPh_3)_2$, (trimethylsilyl)acetylene, TEA, CuI, THF (77%); (xv) **14**, LDA, *n*-pentylpyrazine, THF, −40 °C; (xvi) TBAF, THF (84% for two steps); (xvii) $N_3CH_2(CH_2OCH_2)_2CH_2OTs$, DIPEA, MeCN, CuI, rt (86%); (xviii) NaN_3, DMF, 70 °C (77%); (xix) CH_3I, Cs_2CO_3, DMF (85%); (xx) *p*-TSA, MeOH (84% R = H, 83% R = CH_3); (xxi) H_2, 10%Pd/C, MeOH, rt (64% R = H, 73% R = CH_3).

n-pentylpyrazine. However, all attempts at the Sonogashira reaction with a triethylene glycol-bearing acetylene failed as only the starting materials and/or a diyne product were recovered, presumably due to the incompatibility of the reaction with the TEG chain. Bearing in mind the challenges associated with the synthesis of pyrrolo[2,3-*b*]pyrazine core in the presence of a TEG chain, we turned our attention toward a more efficient conjugation method to introduce the linker. Amongst the common methods reported, the copper(II)-catalyzed 1,3-dipolar cycloaddition between an alkyne and an azide (so-called 'click' chemistry) was investigated. To this aim, the bromobenzonitrile **13** was reacted under Sonogashira conditions with (trimethylsilyl)acetylene to afford the 3-alkynylbenzonitrile **14** in 77% yield. Condensation of **14** with pentylpyrazine using the optimized conditions gave a mixture of **15** and the desilylated product **16**. Further treatment of this mixture with TBAF allowed obtention of pure **16** in 84% over two steps. The cycloaddition step with the tosylate of an azido-substituted triethylene glycol[23] was then performed using CuI and DIPEA in acetonitrile at room temperature and afforded the desired product **17** in 86% yield. Finally, displacement of the tosyl with sodium azide, cleavage of the 4′-OTHP with p-TSA, and reduction of the azide gave the amino-terminated linked aloisine **20**. Using the same strategy, the *N*-methyl analogue **21** was obtained by methylation of **18** prior to reduction.

Incorporating the chain at a late stage by click chemistry overcomes the problems associated with the combination of a basic and hygroscopic pyrrolo[2,3-*b*]pyrazine core and a chelating, hydrophilic TEG, responsible for the often poor yields obtained previously. In view of the well-documented functional group compatibility of both the Sonogashira reaction and the 'click' chemistry, as

Table 1
Kinase inhibition by aloisine A and analogues

Compound tested	Protein kinase IC_{50} (μM)		
	CDK1/cyclinB	CDK5/p25	GSK-3
Aloisine A	0.15	0.20	0.65
N-Methyl-aloisine A	140	160	>200
5	0.23	0.66	0.34
6	100	50	45
20	6.7	>10	5.8
21	>10	>10	>10

well as the high yields obtained, this latter approach provides a more satisfactory solution for the incorporation of TEG chains onto inhibitor structures for the purposes of affinity chromatography.[24]

Before using these PEG extension-linked analogues for affinity chromatography analysis, their inhibitory efficacy on CDK1/CyclinB, CDK5/p25 and GSK-3α/β was tested and compared to aloisine A. The results obtained are presented in Table 1. Introduction of the linker at the 4′-OH of aloisine A (analogue **5**) did not greatly modify the CDK1, CDK5 and GSK-3 inhibition properties. In the case of an addition of the linker at the C-3′ position of aloi-

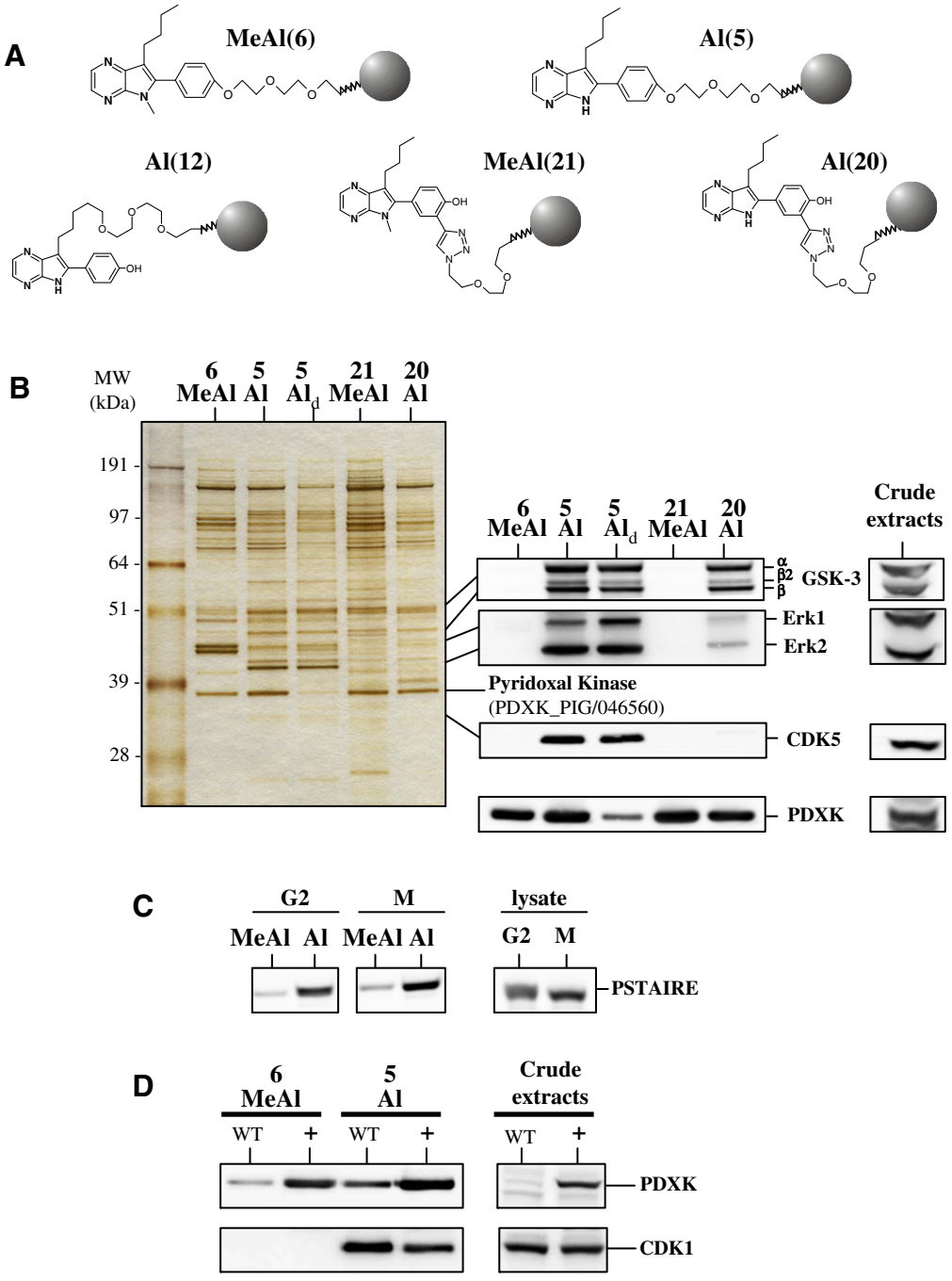

Figure 1. Affinity chromatography purification of the targets of aloisine A. (A) Matrices used in this study. Methyl-aloisine control beads are indicated by **MeAl** followed by the number small chemical compound immobilized (e.g., **MeAl**(**6**)). Aloisine A matrices are indicated by Al followed by the compound number (e.g., **Al**(**5**)). Different compounds correspond to different positions of the linker chain. Extracts from porcine brain (B), and starfish G2 and M phase oocytes (C) HEK293 cells overexpressing (**+**) or not (WT) the human PDXK (D) were incubated with immobilized-drug matrices. After extensive washing, the affinity matrix-bound proteins were resolved by SDS–PAGE. The identification of the proteins detected after silver staining was realized by western blotting with specific antibodies or mass spectrometry in the case of PDXK. The Anti-PSTAIRE antibody cross-reacts with CDK1, CDK2 and CDK3. Concerning the Al_d lane, the porcine brain lysate was depleted on methyl-aloisine beads (**MeAl**(**6**)) before the purification on aloisine beads (**Al**(**5**)).

sine A (analogue **20**), the inhibition properties are significantly decreased. This modification is probably the consequence of steric hindrance inside the ATP binding pocket of the selected kinases. As already known,[18] the substitution of the hydrogen atom in position 5 by a methyl group results in a dramatic decrease in the inhibitory activity of the analogues **6** and **21**. The aloisine A analogues **5** and **6** were thus chosen as the best tools for the initial selectivity analysis by affinity chromatography. However, the remaining analogues were used for identifying cellular targets that bind in a different manner than the CDK's.

2.2.4. Preparation of affinity chromatography matrices

In order to identify the cellular targets of aloisine A, the chemical analogues substituted with a linker at the different positions (compounds **5** and **6**, **12**, **20** and **21** in Scheme 2) were coupled to sepharose beads to provide the matrices **Al(5)**, **MeAl(6)**, **Al(12)**, **Al(20)**, and **MeAl(21)** (Fig. 1A). Coupling of the compounds to the matrix were realized according to the recommendations of the manufacturer (Sigma–Aldrich) and is described in the experimental procedures section. Sepharose beads conjugated with ethanolamine were prepared as controls.

2.3. Identification of potential cellular targets of aloisine A

2.3.1. Purification of potential aloisine A cellular targets by affinity chromatography

The immobilized small-molecule ligand matrices were first incubated with porcine brain extracts. Unbound proteins were subsequently removed in a series of washing steps, and specifically bound proteins were eluted using SDS–PAGE sample buffer to disrupt the interaction between the target proteins and the immobilized small-molecule ligand. Finally, proteins were identified by immunodetection (Fig. 1B) or by mass spectrometry (Fig. 2).

Methyl-aloisine is unable to form the canonical hydrogen bond pair with the hinge region in the ATP-binding site of protein kinases,[25] and can thus be used in biological studies as a control for those effects not related to protein kinases. It is therefore of interest to focus on those bands that are absent from methyl-aloisine control beads **MeAl(6)** but present on the aloisine A matrix Al(**5**). Thus it is possible to reduce the complexity of the profile obtained by depletion of the porcine brain lysates on control beads (lane $\mathbf{Al_d}$). Under these experimental conditions, the purified proteins are related to those biological activities of aloisine A that would not be observed with the methyl-aloisine A as a negative control. As expected, confirming the selectivity analysis of Mettey et al.[18] using a panel of 26 different protein kinases, CDK5, GSK-3α, GSK-3β and β2 (a splicing isoform of GSK-3β[26]) and also ERK1 and ERK2, were purified on aloisine A beads. Using starfish oocyte lysates at G2 and M phases of the cell division cycle, we showed also that CDK1 can bind to the aloisine A matrix **Al(5)** (Fig. 1C). Only a very small amount of CDK1 was detected on the methyl-aloisine matrix **MeAl**(**6**).

Three other matrices, **Al(12)** and **Al(20)**, and **MeAl(21)** sepharose beads, were used in this study to evaluate the influence of the linker position on the chromatographic process. The matrix bearing the aloisine analog **Al**(**12**) with the linker on the C-7

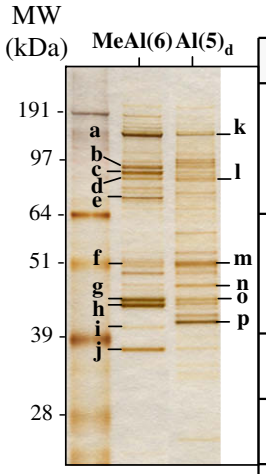

MeAl(6) beads	$\mathbf{Al(5)_d}$ matrix
a. Clathrin heavy chain 1 (CLH1_Human) and Glycogen Debranching Enzyme (GDE_CANFA)	**k.** Clathrin heavy chain 1 (CLH1_Human)
b. Exportin 1 (XP01_HUMAN), Exportin 7 (XP07_PONPY) and Oxoglutarate dehydrogenase (ODO1_Human)	**l.** Glycogen phosphorylase (PYGM_BOVIN)
c. Exportin 2 (XP02_HUMAN)	**m.** Tubulin and GSK-3α (GSK3a_HUMAN)
d. Glycogen phosphorylase (PYGM_BOVIN)	**n.** GSK-3β (GSK-3b_HUMAN)
e. Fuse binding protein 1 (FUBP1_MOUSE)	**o.** MAPK3 (ERK1) (MK03_MOUSE)
f. Tubulin beta chain (TBB_PIG)	**p.** MAPK1 (ERK2) (MK01_RAT)
g. Glutamine synthase (GLNA_PIG)	
h. Glutamine synthase (GLNA_PIG) and beta Actine (ACTB_CERPY)	
i. Glial Fibrillary acidic protein (GFQP_BOVIN)	
j. Pyridoxal kinase (PDXK_PIG)	

Figure 2. Aloisine A can bind different protein kinases and pyridoxal kinase but also various other classes of cellular proteins. Porcine brain lysates were subjected to affinity chromatography purification on **MeAl**(**6**) beads or on **Al**(**5**) beads. In the latter case, the lysate was first depleted on **MeAl**(**6**) methyl-aloisine beads as described in the legend of Figure 1. Gel was stained and the major bands were excised and analyzed by mass spectrometry. The results of this analysis are reported in the table. The proteins were identified using MALDI-TOF peptide mass fingerprint mapping, thus the accession codes indicate the closest protein sequences in the databases (the genome of the pig (*Sus scrofa*) is currently only partially sequenced). Mowse scores, sequence coverages, calculated masses, and additional data using heavier loading are provided in the Supplementary data.

position did not show any specific binding and gave results identical to the ethanolamine control (not shown). As shown in Figure 1, the matrix **Al(20)** with a C-4′ linker cannot bind CDK5 but can bind GSK-3. This is most likely due to steric hindrance. Indeed, the study of the binding mode of CDKs/GSK-3 inhibitors by co-crystallization experiments have indicated that the major difference is located in the entrance of the ATP-binding pocket and thus that GSK-3 can accommodate bulkier compounds compared to CDK5.[27,28] The result obtained for the inhibition of GSK-3 by **20** confirms this data (see Table 1). Indeed compound **20** is still able to inhibit the GSK-3 kinase activity (IC_{50} = 5.8 μM) but less efficiently than compound **5** (IC_{50} = 0.34 μM). This indicates also that modification of the structure at this position by addition of bulky group could be used to increase the selectivity of aloisines for GSK-3. In addition, a band that corresponds to a ~37 kDa protein is detected on all the matrices evaluated. This band was excised from the gel for identification by mass spectrometry and corresponds to the porcine pyridoxal kinase, PDXK. We further confirmed this interaction with human PDXK stably over-expressed in human HEK293 cells (Fig. 1D). In this case, the high level of PDXK expression results in reduced binding of CDK1, suggesting a competition for binding to aloisine. PDXK may thus act as a sink for aloisine and cells over-expressing PDXK may thus lose some sensitivity to aloisine. As expected, the methyl-aloisine gel **MeAl(21)** did not bind GSK-3, but does bind PDXK.

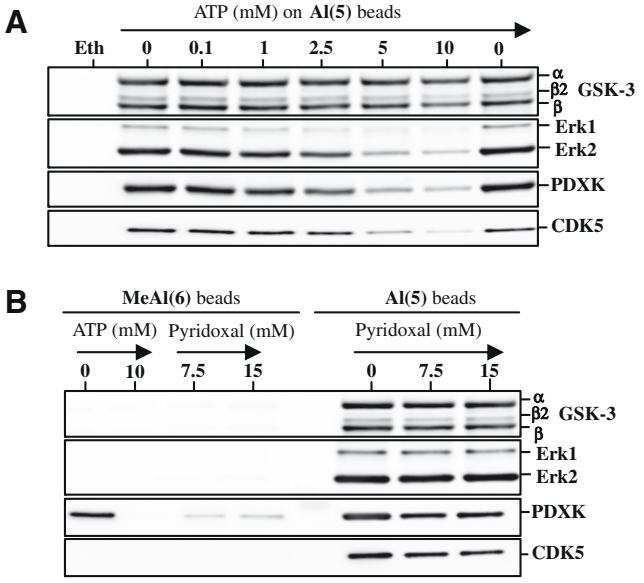

Figure 3. Analysis of the mode of interaction between cellular components and affinity matrices by competition assays. Porcine brain extracts were supplemented with increasing concentrations of ATP (A and B) or pyridoxal (B), prior to loading on the indicated matrices (**Al**(**5**) or **MeAl**(**6**)).

2.3.2. Identification of potential cellular targets by MALDI-TOF mass spectrometry

Eleven bands obtained from the **MeAl(6)** and 12 bands obtained from methylaloisine-depleted **Al(5)** matrices were excised and analyzed by MALDI-TOF peptide mass fingerprint mapping. The bands that yielded conclusive identifications are reported in Figure 2. All the mass spectrometry data obtained are reported in the S1 (for **MeAl(6)** matrix) and S2 and S3 (for **Al(5)** matrix) tables of the Supplementary data section.

Methyl-aloisine A interacts with several classes of non-kinase proteins. The methyl-aloisine A matrix **MeAl(6)** binds notably to: (i) glycogen debranching enzyme that helps facilitate the breakdown of glycogen;[29] (ii) oxoglutarate dehydrogenase, a key control point in the citric acid cycle that uses NADP+ and coenzyme A as co-factors;[30] (iii) glycogen phosphorylase, catalyzes phosphorolytic cleavage of the α(1→4) glycosidic linkages of glycogen and uses pyridoxal phosphate for acid/base catalysis by the enzyme, which furthermore has a well characterized indole-binding site;[31] iv) fuse binding protein 1 that has been shown to function as an ATP-dependent DNA helicase;[32] (v) glutamine synthase, an enzyme that plays an essential role in the metabolism of nitrogen by catalyzing the condensation of glutamate and ammonia to form glutamine in the presence of ATP.[33]

Similar analysis of protein bands on the parent aloisine matrix **Al(5)** after depletion on the **MeAl(6)** matrix (Fig. 2) confirm the immunoblot results in Figure 1: both GSK-3 and Erk isoforms were identified by peptide mass fingerprint mapping. Removing more abundant and less selective targets by depletion on the **MeAl(6)** matrix will permit to better identify less abundant targets such as protein kinases, and to focus on those targets that rely on the canonical ATP-competitive H-bonding pattern. However, no additional targets bound on the depleted **Al**(**5**) inhibitor matrix were identified, with the exception of tubulin, glycogen phosphorylase and clathrin heavy chain 1, all of which were also identified on the **MeAl**(**6**) matrix.[34] Heavier loading of the matrix in order to study some of the minor bands led only to the identification of weakly binding, relatively abundant metabolic proteins (Table S3 of the Supplementary data), but no additional protein kinases.

2.3.3. Mode of binding of aloisine and methyl-aloisine to their putative cellular targets

In order to analyse the mode of binding of aloisine and methyl-aloisine, we have analyzed the effect of increasing the concentrations of ATP and pyridoxal in the brain extract, prior to and during incubation with aloisine beads, on the binding of several protein targets (Fig. 3). First, ATP is able to compete for the binding of GSK-3 isoforms, ERK1/2, PDXK and CDK5 to **Al(5)** beads (Fig. 3A). These results are consistent with kinetic studies, as well as the resolution of a CDK2-aloisine co-crystal structure, that demonstrate that aloisine acts by competitive inhibition of ATP binding to the catalytic subunit of protein kinase.[18] In the case of PDXK the mode of interaction is less predictable. ATP is able to compete for the binding of PDXK to both **Al(5)** beads and **MeAl(6)** beads (Fig. 3A and B). Pyridoxal can only compete for the binding of PDXK to the **MeAl**(**6**) matrix (Fig. 3B) beads suggesting that methyl-aloisine A and aloisine A have two different binding sites on pyridoxal kinase.

2.4. Aloisine A inhibition of non-mammalian targets

2.4.1. Aloisine A inhibits two budding yeast CDKs

There are six CDKs in the budding yeast *Saccharomyces cerevisiae*. Among these CDKs are Cdc28 and Pho85 that bind two distinct classes of cyclins to perform different functions namely regulation of the cell cycle transitions (Cdc28) or regulation of the cellular response to nutrient levels and environmental conditions (Pho85).[35] Pho85 is the yeast functional homologue of the mammalian CDK5[36] and is the most closely related kinase in the yeast kinome to Cdc28 (for review see[37]). Cdc28 is the yeast homologue of CDK1 and regulates each cell cycle transition in yeast.[38] As shown in Figure 4A, both Pho85 and Cdc28 can be purified on aloisine matrix from yeast cell lysates. As expected, methyl-aloisine cannot bind to these CDKs. To confirm these targets, we have analyzed the inhibition of Pho85 and Cdc28. An in vivo assay using the transcription factor Pho4 tagged with GFP was used to analyse the effect on Pho85 (the principle is described in the legend of Fig. 4). A 250 μM aloisine treatment induces a nuclear localization of the GFP-tagged transcription factor Pho4 showing that Pho85 is

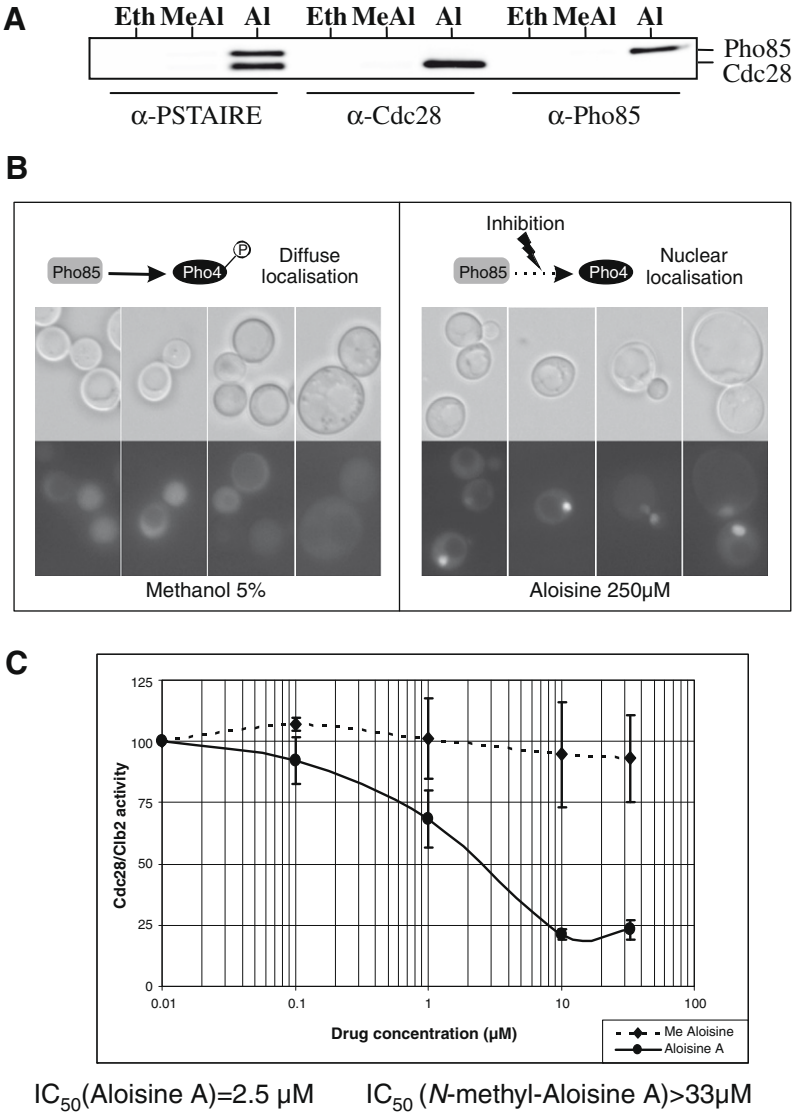

Figure 4. Aloisine A can bind and inhibit Cdc28 and Pho85 yeast CDKs. (A) Extracts from budding yeast *Saccharomyces cerevisiae* were incubated with immobilized-drug matrices **MeAl**(**6**) and **Al**(**5**). A control matrix, sepharose beads quenched with ethanolamine, was used (**Eth**). After extensive washings, the affinity matrix-bound proteins were resolved by SDS–PAGE. The identification of the proteins was realized by western blotting with specific antibodies. Note that both Pho85 and Cdc28 primary sequences have the PSTAIRE motif. (B) The transcription factor Pho4 is one of the Pho85 substrates. Its phosphorylation by Pho85 triggers its export from the nucleus by the receptor Msn5. Therefore, when Pho85 is inhibited, the absence of phosphate leads to a Pho4 nuclear localization. Using a GFP tag, it provides a sensitive fluorescence-based assay to follow inhibition of Pho85 (assay described in[39]). The treatment of yeast cells with aloisine A (right panel) leads to a significant nuclear localization of Pho4-GFP. Note that the treatment with methanol (solvent of the drug in this assay) does not modify the localization (left panel). (C) Cdc28/Clb2 activity was assayed in the presence of increasing concentrations of methyl-aloisine and aloisine A. Kinase activities are expressed as a % of the maximal activity that is measured in the absence of inhibitor.

inactive in presence of the drug, whereas 5% methanol (solvent of the drug used in this study) does not affect the localization. Concerning Cdc28, the active kinase was purified by immunoprecipitation using anti-HA antibody and was used for the determination of the IC_{50} of both aloisine A and methyl-aloisine A (Fig. 4C). The IC_{50} for aloisine A is 2.5 μM, and, as expected, methyl-aloisine cannot inhibit Cdc28/Clb2. Cdc28 is essential for yeast and inhibition of its activity leads to cell cycle arrest and thus to growth defect that can be easily observed on agar plate using halo assay.[39] We have tested the ability of aloisine A to inhibit the yeast growth. Even using a drug-sensitized yeast strain, no growth defect was observed following treatment of cells with aloisine A, suggesting that aloisine A may not enter yeast cell very well. This can explain the relative high concentration needed (250 μM) to observe a phenotype in the Pho85 functional assay. It remains difficult to precisely evaluate the concentrations of small molecules within cells due to the numerous and complex factors involved (permeability, efflux, subcellular localization, etc.).[39]

2.4.2. Aloisine A inhibits the *Plasmodium falciparum* homologue of GSK-3

Increasing resistance worldwide of *P. falciparum* to common anti-malaria agents calls for the urgent identification of new drugs. The perspective is now to identify new molecular targets which could be screened for selective and potent inhibitors of a physiological process essential to the parasite. Among the estimated 6000 genes of *P. falciparum*, protein kinases constitute attractive candidates as potential targets (see review in ref.[40]). Using *P. falciparum* extracts obtained during the red blood cell stage of the infection, the *Pf*GSK-3 was bound onto aloisine A matrix (Fig. 5A). *Pf*GSK-3 shares a high degree of similarity with human GSK-3.[41] This direct interaction with aloisine matrix was

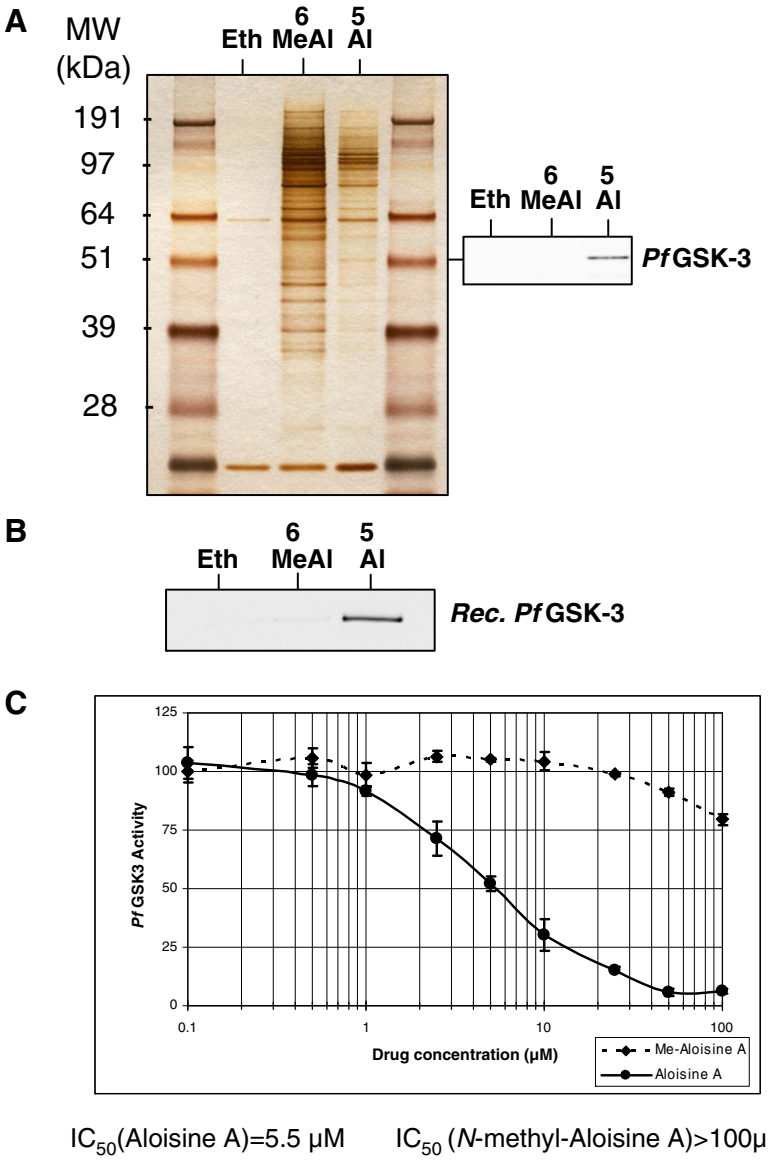

Figure 5. Aloisine A can bind and inhibit GSK-3 from *Plasmodium falciparum*. (A) *Plasmodium falciparum* lysates obtained during the red blood cell stage of the infection were subjected to affinity chromatography purification on ethanolamine (**Eth**), methyl-aloisine (**MeAl**(**6**)) or aloisine (**Al**(**5**)) beads. The identification of the band corresponding to *Pf*GSK-3 on the silver-stained gel was realized by Western blotting with specific antibody. Note that all the major protein bands detected on aloisine A matrix by silver staining of the polyacrylamide gel are also present on methyl-aloisine beads. (B) A recombinant *Pf*GSK-3 can bind to the aloisine matrix. C, *Pf*GSK-3 recombinant enzyme can be inhibited by aloisine with an IC_{50} of 5.5 μM. Note that methyl-aloisine A cannot inhibit recombinant *Pf*GSK-3 enzymatic activity. Kinase activities are expressed in% of maximal activity.

confirmed using recombinant *Pf*GSK-3 produced in bacteria (Fig. 5B). *Pf*GSK-3 recombinant enzyme can be inhibited by aloisine with an IC_{50} of 5.5 μM. Aloisine is thus considered as a new inhibitor of *Pf*GSK-3 although it is 8.5-fold less potent than on mammalian GSK-3 (Table 1).

3. Discussion

Aloisine A (7-*n*-butyl-6-(4′-hydroxyphenyl)-5*H*-pyrrolo[2,3-*b*] pyrazine) is a potent inhibitor of different protein kinases. Prior to this study, its specificity was known essentially from its in vitro effect on fewer than 30 protein kinases. Such an assay only reflects a part of the 518+ kinases that constitute the human kinome, but indicates that aloisine A appears to be remarkably specific to CDK1/2/5 and GSK-3.[18] The current study shows that despite the relative selectivity of aloisine for CDKs and GSK-3, aloisine can also bind to other kinds of cellular proteins and notably to PDXK.

These results show that PDXK could be considered as a frequent off-target of small chemical inhibitors of CDKs. Indeed, a recent study has shown the interaction of (*R*)-roscovitine with PDXK.[17,42] This drug is frequently studied and used as a CDK inhibitor. Like aloisine A, it inhibits protein kinases by direct competition with ATP for binding to the catalytic cleft (reviewed in Ref. 43). Concerning the interaction with PDXK, co-crystal structures showed that roscovitine occupies the ATP-pyridoxal binding groove. Interestingly, roscovitine is not directly binding at the ATP site, but at the pyridoxal site.[42] The authors showed that both ATP and pyridoxal can compete for the binding of PDXK to roscovitine affinity matrix.[17] Thus our data indicate that methyl-aloisine seems to share the same mode of binding. In the case of aloisine A, we can suggest that the small chemical compound may use the ATP

binding site. A co-crystal structure of PDXK-aloisine A would clearly shed light on the position of atoms involved in the interaction. These data would be helpful to obtain derived structures of aloisine that cannot bind to PDXK but still to protein kinases to avoid potential side effects during preclinical/clinical studies. Indeed, PDXK catalyses the phosphorylation of the three forms of vitamin B6 (pyridoxine, pyridoxal and pyridoxamine) in the presence of ATP and Zn^{2+}. This phosphorylation constitutes an essential step in the synthesis of pyridoxal 5′-phosphate, the intracellular active form of vitamine B6, a key factor for at least 140 enzymes, such as aminotransferases and decarboxylases. But, in the case of the roscovitine, despite the interaction of this drug with PDXK, its effects on the catalytic activity of PDXK are rather limited. Experimental data indicate that only 100 μM of ATP is sufficient to compete roscovitine out, therefore resulting in a weak effect on PDXK activity.[42]

This study of putative cellular targets of aloisine and methyl-aloisine using an affinity chromatography method has further shown that these compounds can also interact with non kinase proteins: for instance glycogen phosphorylase, glycogen-debranching enzyme, oxoglutarate dehydrogenase, glutamine synthase, and Fuse binding protein 1. We feel that these findings illustrate the advantages of this method for identifying cellular targets of a given family of compounds. Indeed, these results were unexpected before this study and can only be obtained using such a comprehensive approach. However, these results must still be analyzed carefully in order to evaluate the contribution of the binding of aloisine A to these proteins to the pharmacological properties of the drug, such as the inhibition of cell proliferation as shown by Mettey et al.[18] The use of methyl-aloisine as a negative control in such studies, however, can help restrict the origin of the observed effect to the protein kinases that were identified after depletion on the **MeAl**(**6**) matrix (**Al_d**), namely the CDK, ERK and GSK isoforms.

Using various models, from unicellular eukaryote to mammalian cells and tissues, we have also shown the conservation of targets of aloisine A through evolution, as illustrated by the inhibition of two budding yeast CDKs (Pho85 and Cdc28), and also the GSK-3 counterpart of *P. falciparum*.

The simultaneous evaluation of all classes of proteins expressed in one tissue (from dehydrogenases to protein kinases) is one of the strengths of this method. But as such, it also raises the question of the relative expression of the putative targets. Indeed, this method reflects the distribution of the inhibitor within target proteins in the cell, meaning that highly abundant detected targets can mask less abundant, though perhaps relevant candidates. In our case, we chose to focus on those targets that do not bind the methyl-aloisine negative control by depleting the cell lysates on the methyl-aloisine matrix. For the most part these were limited to the expected CDK, GSK-3 and ERK isoforms. It is particularly interesting to note that the off-target activities of the aloisines are *not* due to the typical ATP-competitive binding mode, as these targets all bind equally well to methyl-aloisine.

It is also worth pointing out here that while these matrices could be used to provide a comprehensive determination of all cellular targets (preferably using human tissues), it is not the objective of the current study. Larger amounts of proteins and matrix associated with separation of the putative targets using two-dimensional gel electrophoresis have been used to increase the sensitivity of the analysis in the study of chemical inhibitors.[44,45] Instead, we aim here to provide only those new targets that were identified conclusively, and an insight into the distribution of the compound among its principal cellular targets. Furthermore, in conjunction with other such studies,[13–17,46] we hope to identify those recurring targets, such as PDXK and NADH-dependent enzymes, that should be included systematically in the panel of enzymes used for the study of protein kinase inhibitor selectivity.

4. Conclusion

Potential applications of CDK/GSK-3 inhibitors are currently evaluated against cancers, neurodegenerative disorders such as Alzheimer's disease, proliferation of protozoan parasites, and viral infections (HIV, cytomegalovirus, and herpes virus). Using affinity chromatography on immobilized drug, we show here the characterization of the putative cellular targets of aloisine A. This compound was initially selected for its ability to be a potent inhibitor of CDK1/2/5 and GSK-3. This study indicates that despite the relative selectivity of aloisine for CDKs and GSK-3, aloisine can also bind to other kind of cellular proteins and notably PDXK. Analysis of various biological models indicates that aloisine selectivity profile is well conserved from the yeast *S. cerevisiae* to human. Each of these interactions must be carefully investigated in order to improve the biological activity of the drug and also to evaluate and avoid the possible side effects preliminary to further assays on animal models of human diseases involving CDK5 and/or GSK-3. However, our results indicate that methyl-aloisine can be used effectively as a control for many of these non-kinase activities.

5. Experimental procedures

5.1. Synthesis

Compounds **2–21** were synthesised by following the pathway described in Scheme 2. Detailed synthetic procedures and spectroscopic data are available in the Supplementary data.

5.2. Affinity chromatography on immobilized drugs

Homogenization buffer: 60 mM β-glycerophosphate, 15 mM *p*-nitrophenylphosphate, 25 mM Mops (pH 7.2), 15 mM EGTA, 15 mM $MgCl_2$, 1 mM DTT, 1 mM sodium vanadate, 1 mM NaF, 1 mM phenylphosphate, 10 μg leupeptin/ml, 10 μg aprotinin/ml, 10 μg soybean trypsin inhibitor/ml and 100 μM benzamidine.

Bead buffer: 50 mM Tris pH 7.4, 5 mM NaF, 250 mM NaCl, 5 mM EDTA, 5 mM EGTA, 0.1% NP-40, 10 μg/ml of leupeptin, aprotinin and soybean trypsin inhibitor and 100 μM benzamidine.

5.2.1. Immobilization of drugs on sepharose matrix

The drug attached to the linker (e.g., **5** for active aloisine; **6** for negative control *N*-methyl analogue) are coupled in 0.1 M $NaHCO_3$, 0.2 M NaCl, pH 8.3 on CNBr-Activated Sepharose 4B (Sigma–Aldrich, #C9142) under agitation at room temperature for 8 h. The final calculated loading was 3 μmol/ml of resin. After the coupling process, the remaining active groups are blocked in pH 8.0 buffer containing 1 M ethanolamine, under agitation for 3 h at 20 °C. The beads are then washed three times with bead buffer and stored in bead buffer (supplemented with 0.05% NaN_3 to avoid microbial growth) at 4 °C until use.

5.2.2. Preparation of extracts

Pork brains were obtained from a local slaughterhouse and directly homogenized and processed for affinity chromatography or stored at −80 °C prior to use. Tissues were weighed, homogenized and sonicated in homogenization buffer (2 ml per g of material). Homogenates were centrifuged for 10 min at 14,000*g* at 4 °C. The supernatant was recovered, assayed for protein content (Bio-Rad protein assay) and immediately loaded batch wise on the affinity matrix. Yeast *S. cerevisiae* extracts were prepared using a 'One Shot' cell disrupter (Constant Systems LTD, Daventry, England).

5.2.3. Affinity chromatography of aloisine-interacting proteins

Just before use, 10 μl of packed aloisine beads were washed with 1 ml of bead buffer and resuspended in 600 μl of this buffer.

The cell or tissue extract supernatant (3 mg total protein) or purified protein was then added; the tubes were rotated at 4 °C for 30 min. After a brief spin at 10,000*g* and removal of the supernatant, the beads were washed 4 times with bead buffer before addition of 60 µl 2X Laemmli sample buffer. Following heat denaturation for 3 min, the bound proteins were analyzed by SDS–PAGE and western blotting or silver staining as described below.

5.2.4. Electrophoresis, western blotting, and silver staining

Following heat denaturation for 3 min, the proteins bound to the aloisine matrices were separated by 10% SDS–PAGE (1 mm thick gels) followed by immunoblotting analysis or silver staining using a GE Healthcare SDS–PAGE silver staining kit. For immunoblotting, proteins were transferred to 0.45 µm nitrocellulose filters (Schleicher and Schuell). These were blocked with 5% low fat milk in Tris-Buffered Saline—Tween-20, incubated for 1 h with antibodies and analyzed by Enhanced Chemiluminescence (ECL, GE Healthcare). The following antibodies were used: anti-GSK-3 (1:1000, Stressgen), anti-CDK5 (1:500; Santa Cruz), anti-ERK1/2 (1:4000; Sigma), anti-p35/p25 (1:500; Santa Cruz), anti-PSTAIRE (1:3000, Sigma), anti-PDXK (1:500;[17]), anti-Pho85 and anti-Cdc28 (respectively given by E. O'Shea and C. Mann).

5.2.5. Protein identification by mass spectrometry

Silver stained protein bands were excised from the corresponding 1D gel. *In-gel* digestion was carried out using porcine trypsin from Promega (Madison, WI, USA): Gel fragments were washed with 2 × 200 µl of 25 mM ammonium hydrogen carbonate, dried with CH_3CN, and dehydrated under vacuum. Then, 10 µl of trypsin solution (12.5 ng/µl in 25 mM ammonium hydrogen carbonate) was added and the digestion was carried out overnight at 37 °C. After separation of the supernatant, gel fragments were washed twice with 50 µl of H_2O/ACN (v/v) containing 0.5% formic acid. The fractions were concentrated under vacuum and stocked at −20 °C. Prior to analysis on an Ultraflex MALDI-TOF-TOF instrument (Bruker Daltonics, Bremen), the peptides were diluted in 20 µl of H_2O/ACN (v/v) containing 0.5% formic acid. One microliter of the peptide solution was mixed directly onto the target with 1 µl of DHB matrix (10 mg/mL of DHB in H_2O/CH_3OH (v/v)). All peptide mass fingerprint spectra were internally calibrated with the tryptic auto-digestion ions. Identification of proteins was achieved using the Mascot algorithm. Only those bands yielding a correlation factor above 60 and a genomic predicted mass that is consistent with the mass observed on the gel are shown in Figure 2. Mowse scores, sequence coverages, calculated masses, and additional data using a heavier loading are provided in the Supplementary data.

5.3. Protein kinase assays

The description of protein kinase preparations and assays (CDK1/cyclin B, CDK5/p25, GSK-3 and *Pf*GSK-3) is provided in the Supplementary data section.

5.4. Biochemical and genetic experiments using the yeast *S. cerevisiae*

5.4.1. Strains and plasmids

MNY629 is a gift from Marie-Noëlle Simon (IGC, Marseille, France) and allows the expression of CLB2 fused to HA-tag. YRP1 is a gift from Karl Kuchler (Vienna University, Austria) and corresponds to a drug-sensitized yeast strain (*snq2Δpdr5Δerg6Δ*). EB0347 is a gift from Erin O'Shea (Howard Hughes Medical Institute, Harvard University, Cambridge, MA, USA). It contains *PHO4* promoter and the entire *PHO4* ORF fused in-frame to N terminus of GFP on pRS316 plasmid.

5.4.2. Preparation of extracts

Yeast *S. cerevisiae* were grown to $OD_{600nm} \approx 2$ (exponential phase). A yeast pellet is then obtained by centrifugation (3000 rpm, 15 min) and diluted in breaking buffer (25 mM Tris pH 7.4, 100 mM NaCl, 0.2% Triton X100, 15 mM *p*-nitrophenylphosphate, 0.1 mM Na-Vanadate, 1 mM PMSF and protease inhibitor cocktail (CompleteTM, Roche)). Cells were broken using a 'One Shot' cell disrupter (Constant Systems LTD, Daventry, England) with a 2.5 kbar pressure. Extracts were clarified by centrifugation (13,000 rpm, 20 min) before protein quantification using a Bradford assay.

5.4.3. Immunoprecipitation

Protein A/G PLUS-agarose (Santa Cruz, SC-2003) and monoclonal anti-HA (Covance, MMS-101R) were used for immunoprecipitation of the complex Cdc28/Clb2-HA before kinase assay.

5.4.4. Kinase assays

Purified Cdc28/Clb2-HA complex was incubated for 30 min at 30 °C in a 30 µl reaction mix containing 5 µl of Histone H1 (1 mg/ml), 6 µl of [$^{\gamma\text{-}33}$P]ATP (15 µmol/l) and varying concentrations of drugs in buffer C (60 mmol/l β-glycerophosphate, 15 mmol/l *p*-nitrophenylphosphate, 25 mmol/l MOPS (pH, 7.2), 5 mmol/l EGTA, 15 mmol/l MgCl2, 1 mmol/l DTT, 1 mmol/l sodium vanadate, 1 mmol/l phenylphosphate). After 30 min incubation at 30 °C, 20 µl of supernatant were spotted onto pieces of Whatman P81 phosphocellulose paper. The filters were washed three times (for at least 5 min each time) in a 1% phosphoric acid solution. The wet filters were counted in the presence of 1 ml ACS (GE Healthcare) scintillation fluid.

5.4.5. Pho4-GFP assay

YRP1 carrying EB0347 plasmid were grown over-night under selection (w/o uracil) then diluted at $OD_{600nm} = 0.5$. The culture is treated with 250 µM aloisine A. Samples are observed at 3 h and analyzed with fluorescence microscopy: GFP-tagged proteins were visualized using a Chroma GFP4 filter (excitation 455–495 nm) on an Olympus BX61 microscope and photographed with a Diagnostic Instruments Spot RT cooled CCD camera.

Acknowledgments

We thank Dr. E. O'Shea for Pho4-GFP expressing vector and Pho85 antibody, Dr. K. Kuchler for yeast highly permeable strain YRP1 and Dr. M.N. Simon for yeast strains expressing Clb2-HA protein. Special thanks to Dr. C. Mann for Cdc28 antibody and also for helpful suggestions. C.C. and D.G. are doctoral research fellows supported by the 'Région Bretagne—CNRS Département des Sciences du Vivant' and 'Ligue contre le Cancer, Comité des Côtes d'Armor—Association pour la Recherche contre le Cancer', respectively. S.B. is supported by 'Association pour la Recherche contre le Cancer' (Contract ARC No. 3889). This research was also supported by grants from the EEC (FP6-LSHB-CT-2004-503467, PRO-KINASE Research (R.H., L.M., P.G.) and FP6-LSH-2003-2.3.0_2, ANTIMAL (L.M.)) and the Canceropole Grand-Ouest (L.M.).

Supplementary data

Supplementary data (The synthesis and characterization data of compounds **2**–**21**) associated with this article can be found, in the online version, at doi:10.1016/j.bmc.2009.06.024.

References and notes

1. Dhavan, R.; Tsai, L. H. *Nat. Rev. Mol. Cell Biol.* **2001**, *2*, 749.
2. Malumbres, M.; Ortega, S.; Barbacid, M. *Biol. Chem.* **2000**, *381*, 827.

3. Morgan, D. O. *Annu. Rev. Cell Dev. Biol.* **1997**, *13*, 261.
4. Knockaert, M.; Greengard, P.; Meijer, L. *Trends Pharmacol. Sci.* **2002**, *23*, 417.
5. Mazanetz, M. P.; Fischer, P. M. *Nat. Rev. Drug Discovery* **2007**, *6*, 464.
6. Cohen, P. *Nat. Rev. Drug Discovery* **2002**, *1*, 309.
7. Fischer, P. M.; Lane, D. P. *Curr. Med. Chem.* **2000**, *7*, 1213.
8. Gray, N.; Detivaud, L.; Doerig, C.; Meijer, L. *Curr. Med. Chem.* **1999**, *6*, 859.
9. Davies, S. P.; Reddy, H.; Caivano, M.; Cohen, P. *Biochem. J.* **2000**, *351*, 95.
10. Bach, S.; Blondel, M.; Meijer, L.. In *Monographs on Enzyme Inhibitors*; CRC Press: Boca Raton, FL, 2006; Vol. 2, p 103.
11. Terstappen, G. C.; Schlupen, C.; Raggiaschi, R.; Gaviraghi, G. *Nat. Rev. Drug Discovery* **2007**, *6*, 891.
12. Guiffant, D.; Tribouillard, D.; Gug, F.; Galons, H.; Meijer, L.; Blondel, M.; Bach, S. *Biotechnol. J.* **2007**, *2*, 68.
13. Knockaert, M.; Gray, N.; Damiens, E.; Chang, Y. T.; Grellier, P.; Grant, K.; Fergusson, D.; Mottram, J.; Soete, M.; Dubremetz, J. F.; Le Roch, K.; Doerig, C.; Schultz, P.; Meijer, L. *Chem. Biol.* **2000**, *7*, 411.
14. Knockaert, M.; Wieking, K.; Schmitt, S.; Leost, M.; Grant, K. M.; Mottram, J. C.; Kunick, C.; Meijer, L. *J. Biol. Chem.* **2002**, *277*, 25493.
15. Wan, Y.; Hur, W.; Cho, C. Y.; Liu, Y.; Adrian, F. J.; Lozach, O.; Bach, S.; Mayer, T.; Fabbro, D.; Meijer, L.; Gray, N. S. *Chem. Biol.* **2004**, *11*, 247.
16. Brehmer, D.; Greff, Z.; Godl, K.; Blencke, S.; Kurtenbach, A.; Weber, M.; Muller, S.; Klebl, B.; Cotten, M.; Keri, G.; Wissing, J.; Daub, H. *Cancer Res.* **2005**, *65*, 379.
17. Bach, S.; Knockaert, M.; Reinhardt, J.; Lozach, O.; Schmitt, S.; Baratte, B.; Koken, M.; Coburn, S. P.; Tang, L.; Jiang, T.; Liang, D. C.; Galons, H.; Dierick, J. F.; Pinna, L. A.; Meggio, F.; Totzke, F.; Schachtele, C.; Lerman, A. S.; Carnero, A.; Wan, Y.; Gray, N.; Meijer, L. *J. Biol. Chem.* **2005**, *280*, 31208.
18. Mettey, Y.; Gompel, M.; Thomas, V.; Garnier, M.; Leost, M.; Ceballos-Picot, I.; Noble, M.; Endicott, J.; Vierfond, J. M.; Meijer, L. *J. Med. Chem.* **2003**, *46*, 222.
19. Mapelli, M.; Massimiliano, L.; Crovace, C.; Seeliger, M. A.; Tsai, L. H.; Meijer, L.; Musacchio, A. *J. Med. Chem.* **2005**, *48*, 671.
20. Vierfond, J. M.; Mettey, Y.; Mascrier-Demagny, L.; Miocque, M. *Tetrahedron Lett.* **1981**, *22*, 1219.
21. Davis, M.; Wakefield, B.; Wardell, J. *Tetrahedron* **1992**, *48*, 939.
22. Fuchter, M.; Beall, L.; Baum, S.; Montalban, A.; Sakellariou, E.; Mani, N.; Miller, T.; Vesper, B.; White, A.; Williams, D.; Barrett, A.; Hoffman, B. *Tetrahedron* **2005**, *61*, 6115.
23. Eduardo, F. M.; Correa, J.; Irene, R. M.; Ricardo, R. *Macromolecules* **2006**, *39*, 2113.
24. Haddoub, R.; Gueyrard, D.; Goekjian, P. *Tetrahedron Lett.* **2009**, *50*, 741.
25. Traxler, P.; Furet, P. *Pharmacol. Therapeut.* **1999**, *82*, 195.
26. Mukai, F.; Ishiguro, K.; Sano, Y.; Fujita, S. C. *J. Neurochem.* **2002**, *81*, 1073.
27. Fischer, P. M. *Chem. Biol.* **2003**, *10*, 1144.
28. Meijer, L.; Skaltsounis, A. L.; Magiatis, P.; Polychronopoulos, P.; Knockaert, M.; Leost, M.; Ryan, X. P.; Vonica, C. A.; Brivanlou, A.; Dajani, R.; Crovace, C.; Tarricone, C.; Musacchio, A.; Roe, S. M.; Pearl, L.; Greengard, P. *Chem. Biol.* **2003**, *10*, 1255.
29. Watanabe, Y.; Makino, Y.; Omichi, K. *J. Biochem.* **2008**, *143*, 435.
30. Araujo, W. L.; Nunes-Nesi, A.; Trenkamp, S.; Bunik, V. I.; Fernie, A. R. *Plant Physiol.* **2008**, *148*, 1782.
31. Lukacs, C. M.; Oikonomakos, N. G.; Crowther, R. L.; Hong, L.-N.; Kammlott, R. U.; Levin, W.; Li, S.; Liu, C. M.; McGady, D. L.; Pietranico, S.; Reik, L. *Proteins: Structure, Function and Bioinformatics* **2006**, *63*, 1123.
32. Chung, H. J.; Liu, J.; Dundr, M.; Nie, Z.; Sanford, S.; Levens, D. *Mol. Cell. Biol.* **2006**, *26*, 6584.
33. Berlicki, L. *Mini.-Rev. Med. Chem.* **2008**, *8*, 869.
34. Reprocessing of the data with a recent version of the database led to the possible identification of MEK-1 (Table S2 of the Supplementary data). However, Mettey et al. have shown previously that this kinase is not a target of aloisine (Ref. 18).
35. Wu, D.; Dou, X.; Hashmi, S. B.; Osmani, S. A. *J. Biol. Chem.* **2004**, *279*, 37693.
36. Huang, D.; Patrick, G.; Moffat, J.; Tsai, L. H.; Andrews, B. *Proc. Natl. Acad. Sci. U.S.A.* **1999**, *96*, 14445.
37. Huang, D.; Friesen, H.; Andrews, B. *Mol. Microbiol.* **2007**, *66*, 303.
38. Ceccarelli, E.; Mann, C. *J. Biol. Chem.* **2001**, *276*, 41725.
39. Kung, C.; Kenski, D. M.; Krukenberg, K.; Madhani, H. D.; Shokat, K. M. *Chem. Biol.* **2006**, *13*, 399.
40. Doerig, C.; Meijer, L.; Mottram, J. C. *Trends Parasitol.* **2002**, *18*, 366.
41. Droucheau, E.; Primot, A.; Thomas, V.; Mattei, D.; Knockaert, M.; Richardson, C.; Sallicandro, P.; Alano, P.; Jafarshad, A.; Baratte, B.; Kunick, C.; Parzy, D.; Pearl, L.; Doerig, C.; Meijer, L. *Biochim. Biophys. Acta* **2004**, *1697*, 181.
42. Tang, L.; Li, M. H.; Cao, P.; Wang, F.; Chang, W. R.; Bach, S.; Reinhardt, J.; Ferandin, Y.; Galons, H.; Wan, Y.; Gray, N.; Meijer, L.; Jiang, T.; Liang, D. C. *J. Biol. Chem.* **2005**, *280*, 31220.
43. Meijer, L.; Raymond, E. *Acc. Chem. Res.* **2003**, *36*, 417.
44. Godl, K.; Wissing, J.; Kurtenbach, A.; Habenberger, P.; Blencke, S.; Gutbrod, H.; Salassidis, K.; Stein-Gerlach, M.; Missio, A.; Cotten, M.; Daub, H. *Proc. Natl. Acad. Sci. U.S.A.* **2003**, *100*, 15434.
45. Brehmer, D.; Godl, K.; Zech, B.; Wissing, J.; Daub, H. *Mol. Cell. Proteomics* **2004**, *3*, 490.
46. Trapp, J.; Jochum, A.; Meier, R.; Saunders, L.; Marshall, B.; Kunick, C.; Verdin, E.; Goekjian, P.; Sippl, W.; Jung, M. *J. Med. Chem.* **2006**, *49*, 7307.